*Korean J. of Chem. Eng.*, **5**(2) (1988) *190-196*

# A STUDY ON THE NEWTONIAN FLUID FLOW PAST A SPHERE IN A TUBE

**Jang Hoon OH and Seung Jong LEE**

Department of Chemical Engineering, Seoul National University

*(Received 3 March 1988 • accepted 23 June 1988)*

**Abstract**—Newtonian flow past a sphere in a tube of finite radius was investigated experimentally and numerically. The flow visualization technique using He-Ne laser as a light source has been employed to study the vortex characteristics occurring on the backside of the sphere which is set stationary inside the tube moving vertically. It has been revealed that the vortex size decreases as the ratio of sphere to tube diameter ($\alpha$) increases. Galerkin finite element simulation was able to predict those phenomena almost exactly and also used to calculate the drag coefficients which vary with the Reynolds number and $\alpha$.

## INTRODUCTION

The uniform flow past submerged spherical objects is one of the flow situations commonly encountered in many industrial processes. For Newtonian fluids previous works were mostly made on the one in the infinite fluid medium without the wall effect. Taneda[1], Adachi et al.[2] and Brauer[3] performed the flow visualization experiments in a horizontal tank with dimensions $50 \times 50 \times 200$cm. Photographs were taken with a camera which was connected with a sphere and moved at the same speed as the sphere. Vortices depending on the Reynolds number(Re) occurred on the backside of the sphere; i.e., stationary ring vortices for $20 < Re < 130$ and unsteady vortices for $Re > 130$. Here, the Reynolds number(Re) is defined as $\rho DV/\mu$ where $\rho$,D,V and $\mu$ represent the density of the fluid, the diameter of the sphere, the relative velocity of the sphere to the fluid medium and the viscosity of the fluid, respectively.

Numerical solutions have also been obtained by many authors, including Adachi et al.[2], Brauer[3], Jenson[4], Hamielec et al.[5] and Kwon[6].

In this study the flow past a sphere in a tube of finite radius is investigated experimentally and numerically for Newtonian fluids. Main concerns are centered on the vortex characteristics and the drag coefficients affected by the presence of the tube wall.

## EXPERIMENTS

The flow visualization experiments have been carried out to obtain the steady streamlines in the flow past a sphere in a tube. General view of the apparatus is shown in Fig. 1. The unique feature of this apparatus is that the tube containing the whole fluid medium is moving vertically, while the sphere is stationary. Note that in most of previous experimental works the sp-

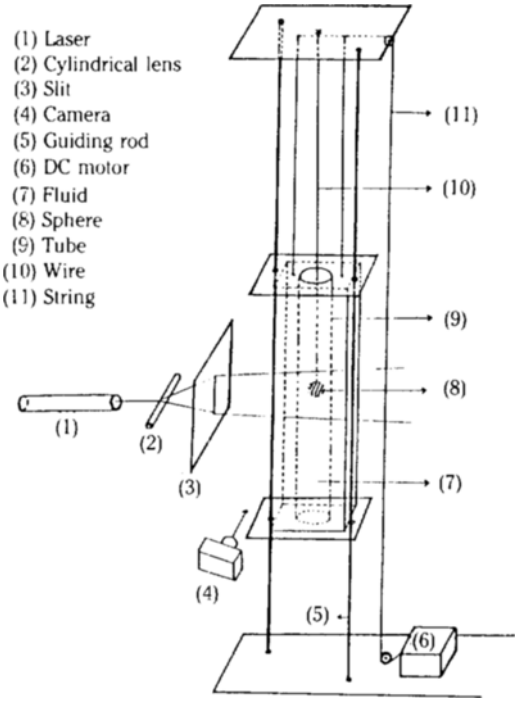


**Fig. 1. Experimental apparatus used for the visualization of the flow past a sphere in a tube.**

here is falling down through the stationary fluid medium. The sphere was set stationary by a thin wire string with diameter of 0.6 mm. It will be discussed later that the effect of this thin wire string becomes negligible. The sphere used in the experiments is made of steel and its diameter was 2.3 cm. The tubes of two different diameters, 3.1 cm and 4.6 cm, were used to investigate the effect of the wall proximity.

The visualization is to illuminate a thin meridian section of the tube after fine bright particles have been suspended uniformly in the fluid, and to photograph the paths of these particles when the tube with length of 90 cm moves downwards. To get steady tube velocity DC motor with variable speed was used. The tube velocity ranged from 0.5 to 7 cm/sec. In order to compensate the diopter effect, the tube was set in the axis of a square acryl-box full of the same fluid as the test fluid. Light from a 10 mW He-Ne laser(NEC Model GLG5340) was spread into a narrow sheet of light by means of a cylindrical lens. This sheet of light was collimated by a slit. A camera to which a close-up ring was attached was used to take photographs. Panatomic-X film (black and white, ASA32) was used and exposure time ranged from 5 to 30 seconds.

## NUMERICAL SIMULATIONS

The finite element analysis of the flow past a sphere in a tube has been carried out to investigate the vortex characteristics observed experimentally and the drag coefficients have been calculated to figure out the effect of the tube wall.

### 1. Governing Equations

Let U(r,z) and V(r,z) denote the radial and axial velocity components in the steady axisymmetric flow, expressed in polar cylindrical (r,z) coordinates. Then, the continuity equation is

$$U_{,r}+U/r+V_{,z}=0 \tag{1}$$

and the momentum equations are

$$\rho(UU_{,r}+VU_{,z})=-P_{,r}+T_{rr,r}+T_{rz,z}+(T_{rr}-T_{\theta\theta})/r+F_r \tag{2a}$$

$$\rho(UV_{,r}+VV_{,z})=-P_{,z}+T_{rz,r}+T_{rz}/r+T_{zz,z}+F_z \tag{2b}$$

where $T_{rr}$, $T_{rz}$, $T_{\theta\theta}$ and $T_{zz}$ are the extra-stress components, P is modified pressure which includes the gravity term, $F_r$, $F_z$ are the components of the body force per unit volume, and a comma followed by subscript r or z denotes partial differentiation with respect to the corresponding variables.

### 2. Galerkin Finite Element Formulation

Let us consider a domain $\Omega$ in the r,z sectional plane bounded by a closed curve $\Gamma$. And let us cover the domain $\Omega$ by a mesh of finite elements, and approximate the unknown velocity components and pressure as follows

$$r=r_i\psi_i(\zeta,\eta) \tag{3a}$$

$$z=z_i\psi_i(\zeta,\eta) \tag{3b}$$

$$U(r,z)=U_j\psi_j(r,z) \tag{4a}$$

$$V(r,z)=V_j\psi_j(r,z) \tag{4b}$$

$$P(r,z)=P_j\phi_j(r,z) \tag{4c}$$

where $\psi_j$'s are the quadractic or biquadratic shape functions and $\phi_j$'s are the linear or bilinear shape functions.

By performing the scalar product of Eqs.(2) with $r\psi_i$ and using the divergence theorem, one finds easily the Galerkin form of the equations of motion.

$$<r\psi_{i,r};-P+T_{rr}>-<r\psi_{i,z};T_{rz}>+<\psi_i;T_{\theta\theta}>-<\psi_i;P>+\rho<r\psi_i;UU_{,r}+VU_{,z}>=<r\psi_i;F_r>+\ll r\psi_i;t_r\gg \tag{5a}$$

$$<r\psi_{i,r};T_{rz}>+<r\psi_{i,z};-P+T_{zz}>+\rho<r\psi_i;UV_{,r}+VV_{,z}>=<r\psi_i;F_z>+\ll r\psi_i;t_z\gg \tag{5b}$$

where $t_r$, $t_z$ are the r and z components of the contact force vector, the notation $<;>$ means the integration over the domain and $\ll\ ;\ \gg$ means the integration along the boundary surface. We now express the extra-stress components in terms of the velocity components to obtain the final form of Galerkin equations.

$$<r\psi_{i,r};-P+2\mu U_{,r}>+<r\psi_{i,z};\mu(U_{,z}+V_{,r})>-<\psi_i;2\mu U/r>-<\psi_i;P>+\rho<r\psi_i;UU_{,r}+VU_{,z}>=<r\psi_i;F_r>+\ll r\psi_i;t_r\gg \tag{6a}$$

$$<r\psi_{i,r};\mu(U_{,z}+V_{,r})>+<r\psi_{i,z};-P+2\mu V_{,z}>+\rho<r\psi_i;UV_{,r}+VV_{,z}>=<r\psi_i;F_z>-\ll r\psi_i;t_z\gg \tag{6b}$$

The Galerkin form of the conservation of mass becomes

$$<r\phi_i;U_{,r}+U/r+V_{,z}>=0 \tag{7}$$

We finally obtain the system of equations by substituting the Eqs.(4) into the Eqs.(6) and (7).

$$(A_{ij}U_j+C_{ij}V_j)+\rho(IR_{ijk}U_jU_k+IZ_{ijk}V_jU_k)-D_{ij}P_j=R_i \tag{8a}$$

$$(C_{ji}U_j+B_{ij}V_j)+\rho(IR_{ijk}U_jV_k+IZ_{ijk}V_jV_k)-E_{ij}P_j=Z_i \tag{8b}$$

$$(-D_{ji}U_j-E_{ji}V_j)=0 \tag{8c}$$

where

$$A_{ij}=2<\mu r\psi_{i,r},\psi_{j,r}>+<\mu r\psi_{i,z};\psi_{j,z}>+2<\mu\psi_i;\psi_j/r> \tag{9a}$$

$$B_{ij} = <\mu r \psi_{i,r}; \psi_{j,r}> + 2 <\mu r \psi_{i,z}; \psi_{j,z}> \quad (9b)$$

$$C_{ij} = <\mu r \psi_{i,z}; \psi_{j,r}> \quad (9c)$$

$$D_{ij} = <r \psi_{i,r}; \phi_j> + <\psi_i; \phi_j> \quad (9d)$$

$$E_{ij} = <r \psi_{i,z}; \phi_j> \quad (9e)$$

$$IR_{ijk} = <r \psi_i; \psi_j \psi_{k,r}> \quad (10a)$$

$$IZ_{ijk} = <r \psi_i; \psi_j \psi_{k,z}> \quad (10b)$$

$$R_i = <r \psi_i; F_r> + \ll r \psi_i; t_r \gg \quad (11a)$$

$$Z_i = <r \psi_i; F_z> + \ll r \psi_i; t_z \gg \quad (11b)$$

The coefficients $A_{ij}$, $B_{ij}$, $C_{ij}$, $D_{ij}$, $E_{ij}$, $IR_{ijk}$, $IZ_{ijk}$ and the right hand sides $R_i$, $Z_i$ in Eqs.(8)-(11) can be obtained by numerical integrations using Gaussian quadrature.

## 3. Meshes and Boundary Conditions

The typical mesh and boundary conditions for solving the system of Eqs.(8) are shown in Fig. 2. The no-slip conditions are applied along the solid wall and the radial velocity(U) and the axial force component($t_z$) vanish along the axis of symmetry. The uniform flat velocity profiles are imposed in the entry and exit sections. The calculations to figure out the effect of thin wire string were also carried out by imposing corresponding geometries and no-slip conditions on the wire surface.

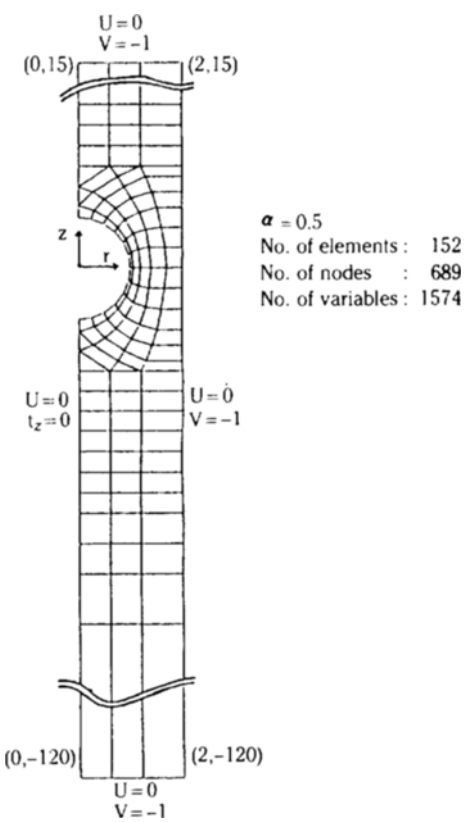


**Fig. 2. Finite element meshes and boundary conditions used when $\alpha = 0.5$.**

## 4. Other Numerical Strategies

Eqs.(8) form a nonlinear system which must be solved by iterative techniques. Newton-Raphson method was used to deal with the nonlinearity and the frontal elimination method[7] was used to reduce the size of stiffness matrix. Convergence of the Newton-Raphson algorithm was remarkably fast. Three or four iterations usually suffice for reaching a relative error of $10^{-4}$. The solutions at lower Reynolds numbers have been used as initial guesses for the calculations at higher Reynolds numbers.

## RESULTS AND DISCUSSION

The effect of the thin wire string which is used to fix the sphere has been first investigated numerically. Fig. 3 shows typical streamlines in the cases with and without wire string. One can easily see that the effect of wire string is negligible as far as the streamlines are concerned. Therefore, in the rest of this paper we present the numerical results without wire string which are compared to the experimental results with the string.

Figs. 4 and 5 show the experimental photographs of the streamlines at various Reynolds numbers for $\alpha$ = 0.5 and 0.74. The dark region is the shadow of the sphere and this shadow could be removed if two laser beams were employed. The dimensionless vortex

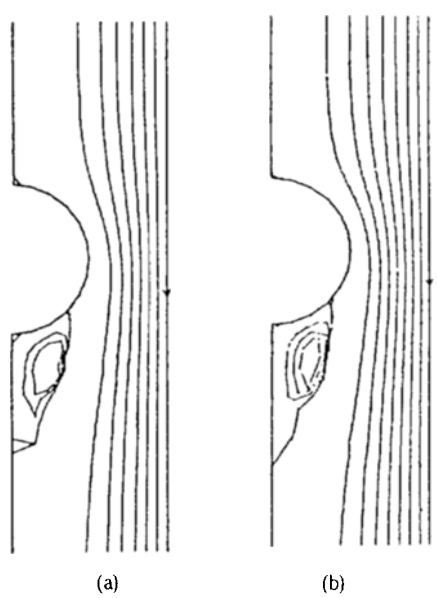


**Fig. 3. The streamlines obtained numerically in the cases (a) with wire string and (b) without wire string for $\alpha = 0.5$ and Re = 100.**

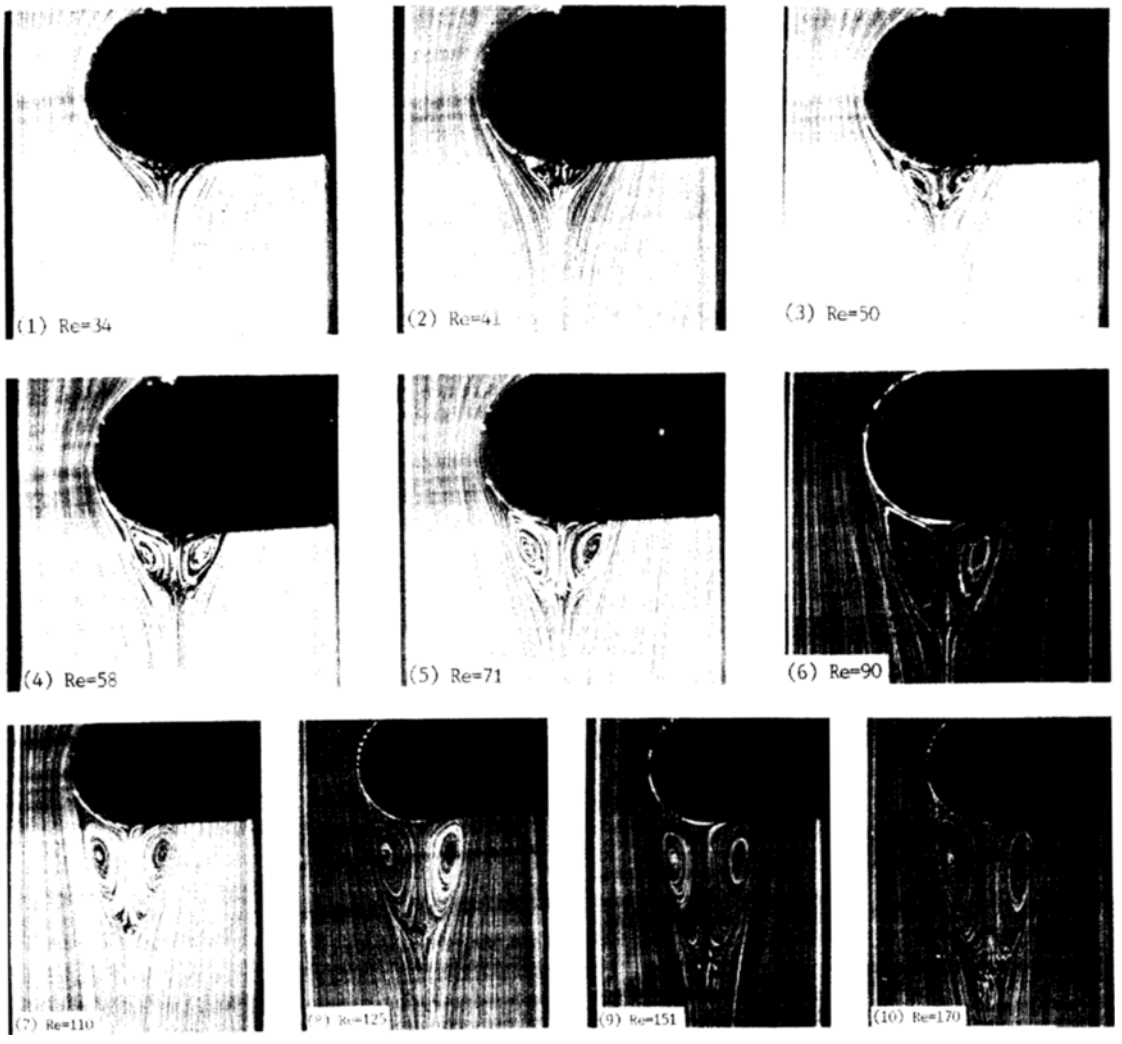


**Fig. 4. Experimental photographs of the streamlines for $\alpha = 0.5$.**

wake(S/R) defined by the ratio of the vortex length to the sphere radius is plotted against Re in Fig. 6, in which S/R obtained numerically is also shown. It is easily found that the dimensionless vortex wake(S/R) increases as Re increases and it decreases as $\alpha$ increases. And the Reynolds number at which the vortex begins to appear increases as $\alpha$ increases and the Reynolds number at which the vortex begins to become unstable also increases as $\alpha$ increases. In Fig. 7 the numerical results are compared to the experimental observations with good agreements.

Next, let us consider the drag coefficient for this system. Once the velocity field is known, the system of Eqs.(8) allows us to calculate the nodal forces on the surface. The sum of the nodal forces in the z-direction multiplied by $2\pi$ gives the drag force(F).Then the drag coefficient $C_D$ is defined as

$$C_D = \frac{F}{1/2\rho V^2 A}$$

where A is the area of the projection of the body on a plane normal to the stream at infinity. In Fig. 8 the drag coefficients calculated numerically are plotted against Re for $\alpha = 0.5$ and 0.74. The previous results of Lapple and Shepherd[8] in infinite fluid medium ($\alpha = 0$) are also shown in Fig. 8. It is seen that the wall proximity increases the drag force on the sphere.

The experimental measurements of the drag force and the studies for the viscoelastic fluid medium are under way.

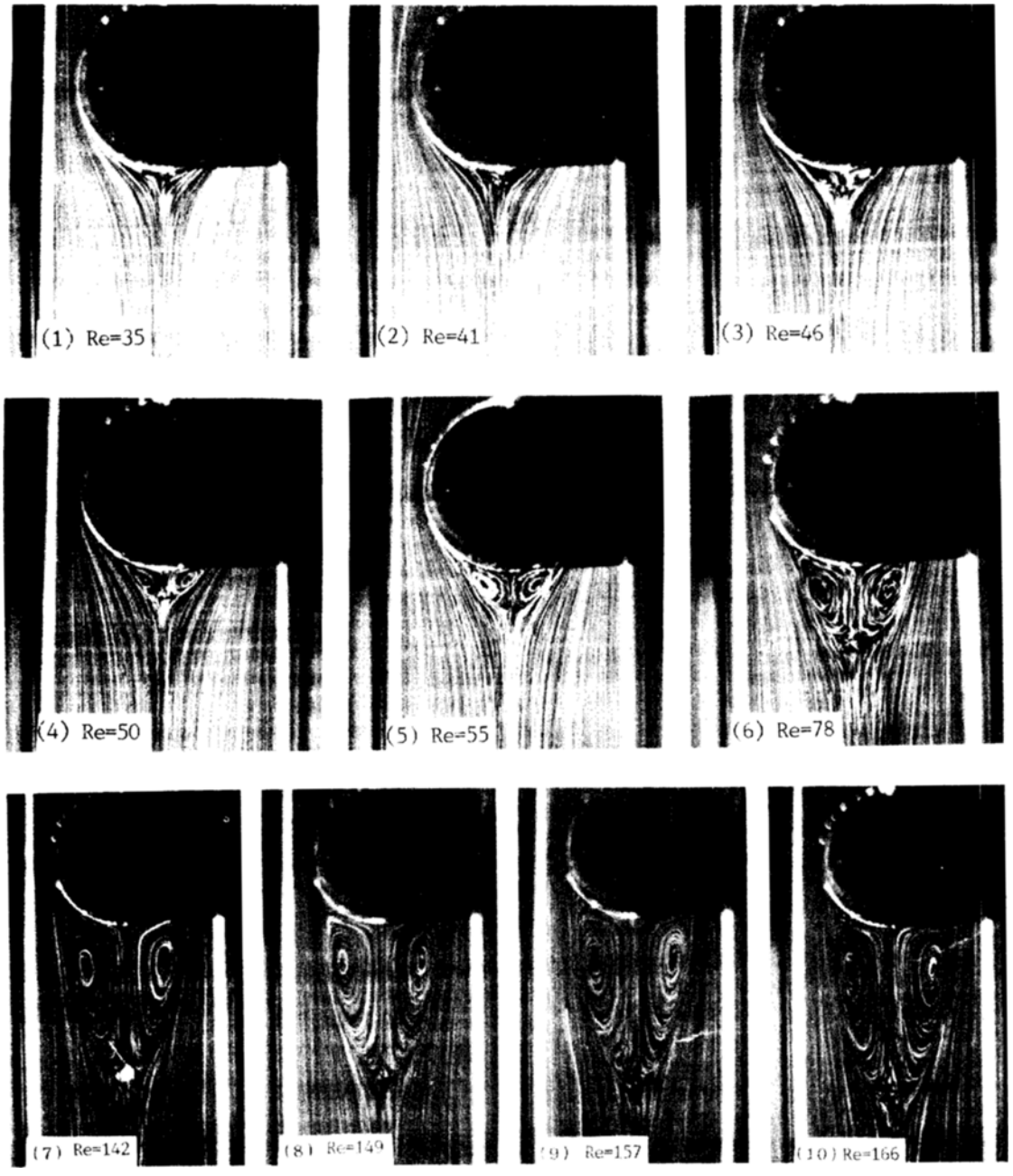


**Fig. 5. Experimental photographs of the streamlines for $\alpha = 0.74$.**

## CONCLUSIONS

The flow past a sphere in a tube of finite radius was investigated experimentally and numerically for Newtonian fluids. The streamlines photographed by the flow visualization experiments and those obtained by the finite elements simulations show good agreements. The size of the vortex occurring on the backside of the sphere increases as Re increases and it decreases as the ratio of sphere to tube diameter($\alpha$) increases. The drag coefficient calculated numerically increases as $\alpha$ increases.

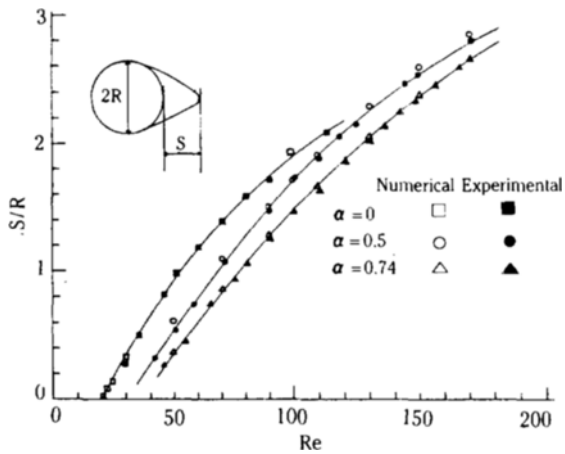


**Fig. 6. The dimensionless vortex wake(S/R) vs. Re at various α.**

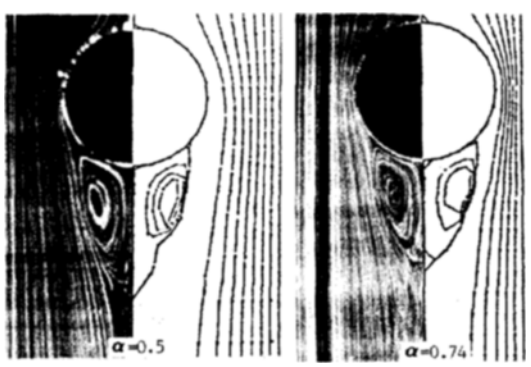


**Fig. 7. Comparison of the streamlines observed experimentally and those obtained by finite element simulations at Re = 100.**

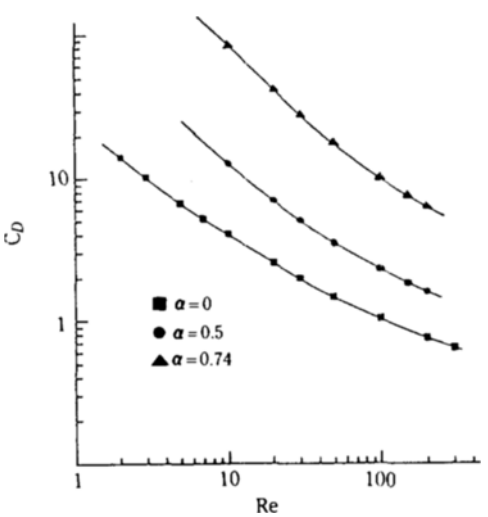


**Fig. 8. The drag coefficients vs. Re at various α.**


## ACKNOWLEDGEMENT

This work was supported by the Korea Science and Engineering Foundation. We are grateful for this support and also for the scholarship from Yukong Ltd. to the first author(J.H.O.).


## NOMENCLATURE

$A_{ij}$ : coefficient matrix
$B_{ij}$ : coefficient matrix
$C_D$ : drag coefficient for flow past a sphere
$C_{ij}$ : coefficient matrix
D : sphere diameter
$D_{ij}$ : coefficient matrix
$E_{ij}$ : coefficient matrix
F : total drag force
$F_r$ : r-component of the body force per unit volume
$F_z$ : z-component of the body force per unit volume
i,j : node indices
P : pressure
$P_j$ : pressure value at node j
Re : Reynolds number
$R_i$ : r-component of right-hand side in Eqn. (8a)
r : radial coordinate in polar cylindrical coordinates
S/R : dimensionless vortex wake length
$T_{ij}$ : extra-stress component
$t_r$ : r-component of the contact force vector
$t_z$ : z-component of the contact force vector
U : radial velocity component
$U_j$ : radial velocity at node j
V : axial velocity component (downward cylinder velocity)
$V_j$ : axial velocity at node j
$Z_i$ : z-component of right-hand side in Eqn. (8b)

### Greek Letters

$\alpha$ : ratio of sphere to cylinder diameter
$\Gamma$ : boundary
$\mu$ : shear viscosity
$\rho$ : density
$\phi_i$ : first-order Lagrangian shape functions
$\psi_i$ : second-order Lagrangian shape functions
$\Omega$ : domain

### Other Symbols

$<;>$ : integration over domain $\Omega$
$\ll;\gg$ : integration along boundary line $\Gamma$

$( )_x$ : partial differentiation with respect to the corresponding variable x

## REFERENCES


1. Taneda, S.: Rep. Inst. Appl. Mech., Kyushu Univ. (Japan), **4,** 99 (1956).
2. Adachi, K., Yoshioka, N. and Skai, K.: *J. Non-Newtonian Fluid Mech.*, **3,** 107 (1977/78).
3. Brauer, H. in A.S. Mujumdar and R.A. Mashelkar (eds.): "Advances in Transport Phenomena", vol. 2, Wiley Eastern Ltd., New Delhi, pp 352-432 (1982).
4. Jenson, V.G.: Proc. Roy. Soc. (London),**A 249,**346 (1959).
5. Hamielec, A.E., Hoffmann, T.W. and Ross, L.L.: *AIChE J.*, **13,** 212 (1967).
6. Kwon, M.H.: M.S. Thesis, Seoul National University (1986).
7. Irons, B.M.: *Int. J. Num. Meth. Eng.*, **2,** 5 (1970).
8. Lapple, C.E. and Shepherd, C.B.: *Ind. Eng. Chem.*, **32,** 605 (1940).